Noncanonical pS727 post translational modification dictates major STAT3 activation and downstream functions in breast cancer

Shalini Dimri, Renu Malhotra, Tanuja Shet, Smruti Mokal, Sudeep Gupta, Abhijit De

PII: S0014-4827(20)30562-0

DOI: https://doi.org/10.1016/j.yexcr.2020.112313

Reference: YEXCR 112313

To appear in: *Experimental Cell Research*

Received Date: 23 April 2020

Revised Date: 15 September 2020

Accepted Date: 27 September 2020

Please cite this article as: S. Dimri, R. Malhotra, T. Shet, S. Mokal, S. Gupta, A. De, Noncanonical pS727 post translational modification dictates major STAT3 activation and downstream functions in breast cancer, *Experimental Cell Research* (2020), doi: https://doi.org/10.1016/j.yexcr.2020.112313.

Author's Credit

Shalini Dimiri – Investigation, Methodology ,Formal analysis, Validation, Visualization, Writing original draft, Review and Editing; **Renu Malhotra** –Investigation, Review and Editing; **Tanuja Shet** – Methodology, Formal analysis, Resources, Review and Editing, **Smruti Mokal**- Software, Formal analysis, Review and Editing; **Sudeep Gupta**- Methodology, Formal analysis, Resources, Review and Editing; **Abhijit De** – Conceptualization, Data Curation, Formal analysis, Funding acquisition, Methodology, Project Administration, Supervision, Writing original draft, Review and Editing.

Noncanonical pS727 post translational modification dictates major STAT3 activation and downstream functions in breast cancer

Shalini Dimri[1,4], Renu Malhotra[1], Tanuja Shet[2,4], Smruti Mokal[2,4], Sudeep Gupta[2,3,4] and Abhijit De[1,4]*

[1]Molecular Functional Imaging Lab, Advanced Centre for Treatment, Research and Education in Cancer, Tata Memorial Centre, Navi Mumbai, INDIA

[2]Tata Memorial Hospital, Mumbai, INDIA

[3]Advanced Centre for Treatment, Research and Education in Cancer, Tata Memorial Centre, Navi Mumbai, India

[4]Homi Bhabha National Institute, Mumbai, INDIA

Running Title: Independent role of noncanonical phosphoS727 STAT3 pathway

***Correspondence:**

Dr. Abhijit De
Molecular Functional Imaging Lab
Advanced Centre for Treatment, Research and Education in Cancer (ACTREC)
Tata Memorial Centre
Sector 22, Kharghar
Navi Mumbai – 410210, India
Phone: +91-22-2740 5038
FAX: +91-22-2740 5085
Email: ade@actrec.gov.in

Authors email addresses:

SD- yashree.dimri@gmail.com; RM- renu_d16@yahoo.com; TS- tanujashet5@gmail.com; SM – smruti272mokal@gmail.com; SG sudeepgupta04@yahoo.com

Abstract

Activation of STAT3 via Y705-phosphorylation is well documented across multiple cancer types and thus forms the basis of canonical pathway to judge STAT3 activation. Recently, important roles of two other post-translational modification (PTM) sites, i.e. S727-phosphorylation and K685-acetylation, leading to STAT3 activation are reported. However, their critical mode of function in controlling STAT3 dimerization and signaling, independent of canonical activation remains elusive. Therefore, to understand the functional relevance of each STAT3 PTMs in breast cancer (BC), cell models are developed by stable overexpression of PTM-site specific point mutants, i.e. Y705F, S727A or K685R, in a 3'UTR-STAT3 knockdown BC cell background. Results using this model system reveal novel findings showing that phosphorylation at S727 can lead to STAT3 activation independent of phosphoY705. We also demonstrate that loss of pS727 or K685ac significantly affects functional phenotypes such as cell survival and proliferation as well as downstream transcriptional activity (Twist 1, Socs3, c-Myc, Bcl-1 and Mcl-1) of STAT3. Thereafter, by utilizing a BRET biosensor for measuring STAT3 phosphorylation in live cells, a crucial role of pS727 in dictating STAT3 activation and homodimerization formation is uncovered. Further by performing retrospective IHC analysis of total and phospho-forms of STAT3 in a cohort of 76 triple negative breast cancer (TNBC) patient samples, a significant dominant expression of phosphoS727 over phosphoY705 PTM ($p<0.001$) is found in STAT3 positive cases**.** We also focus on validating known STAT3 inhibitor molecules for their action against both pY705 and pS727 activation. This study for the first time demonstrates that an anti-helminth drug compound, Niclosamide, is capable of inactivating both phospho-PTM sites on STAT3 and exhibits excellent anticancer efficacy in preclinical TNBC tumour model.

Key Words:

STAT3, Post Translational Modification (PTM), Bioluminescence resonance energy transfer (BRET), Breast cancer, Niclosamide, Triple Negative Breast Cancer (TNBC)

1. Introduction

Signal transducer and activator of transcription 3 (STAT3) is a mediator of cellular signals from cell membrane to the nucleus. In response to soluble cytokines (e.g. IL6, Oncostatin M etc.), hormones (leptin, thrombopoietin etc.) or growth factors (EGF, PDGF etc.), it has been shown over and over that the activated receptors induce phosphorylation of Y705 residue of STAT3 leading to form a homodimer [1, 2]. Once STAT3 dimer forms, it translocate to the nucleus and acts as a transcription factor of key genes involved in oncogenic functions such as cell survival, proliferation, apoptosis, differentiation, angiogenesis and cytokine functions [3, 4]. STAT3 is reported to overexpress in many cancer cell lines and primary tumours such as breast, prostate, head and neck, lung, gastric as well as several haematological malignancies [5, 6]. Literatures clearly suggest that more than 50% of breast cancer (BC) cases are positive for STAT3 overexpression, which plays a pivotal role in disease progression [7-9]. STAT3 is reported to interact with DNMT1 [DNA (cytosine-5)-methyltransferase 1] and methylate the promoter of ERα gene in ER negative BC [10]. Phosphorylation at S727 residue (pS727) of STAT3 is also reported to have negative correlation with the ER status in BC [11]. Also, phosphoY705 activation mark has been identified as a predictive biomarker for invasive BC [12].

Activation of STAT3 via its classical pY705 PTM (i.e. canonical pathway) is well documented and is almost considered synonymous. However, recent reports have shown existence of an alternative activation mechanisms of STAT3 via S727 phosphorylation and K685 acetylation (K685ac), termed as noncanonical pathway [13-15]. Initially pS727 was thought to be required for full transactivation of STAT3 and would occur only after pY705 activation [16]. Recently independent occurrence of pS727 mediated activation of STAT3 is reported, showing that in certain cancer types, STAT3 activation can happen even in the absence of pY705. In chronic lymphocytic leukaemia [17] and ER negative BC [11], pS727 overexpression is observed in tumour tissue even in the absence of pY705 activation and thus affecting cell survival. Predominant expression of pS727 over pY705 STAT3 imparts radiation resistance in glioblastoma that also serves as a predictive marker for poor clinical outcome [18, 19]. On the other hand, acetylated K685 residue was reported to cause STAT3 dimerization and downregulate expression of tumour suppressor genes in breast and ovarian cancer [10, 20]. However, so far there is no investigation done considering canonical and noncanonical STAT3 activation together and hence the possibility of interdependent or independent mode of STAT3 activation by these PTM marks in BC context is not understood.

To study protein homodimer or heterodimer formation in living mammalian cells, bioluminescence resonance energy transfer (BRET) assay has been used for a vast number of endocrine receptor targets as well as cytoplasmic signaling molecules [21-23]. BRET, which follows the Förster energy transfer principle between luciferase donor and fluorophore acceptor, can precisely indicate a definite proximity due to dimer formation. This assay is highly suitable to follow dimerization dynamics in live cell conditions and relays direct influence exerted by varying activator or inhibitor molecules in real time [24-26]. Here, for the first time, we extend the application of our previously developed STAT3 BRET biosensor [27], to analyse phosphorylation of STAT3 mediated by its key PTM marks as a measure of its oncogenic activation.

Therefore, in this comprehensive study we address the significance of canonical vs. noncanonical PTM mediated STAT3 activation in BC. First, by utilizing a robust phospho-BRET sensor platform technology [27], direct evidence of STAT3 dimerization, activation and downstream biological functions is gathered using engineered 3'UTR STAT3 knockdown BC cell line model. After this we verified our *in vitro* observations by performing IHC analysis for total and phospho (pY705 and pS727) STAT3 in 76 paired (pre and post NACT) clinical samples of triple negative breast cancer cases. Considering the importance of the new and clinically relevant understanding developed here, the study is further extended to provide a solution by validating a repurposed drug inhibitor that can effectively block both canonical and noncanonical STAT3 signaling and show potential anticancer effect on preclinical breast cancer model.

2. Materials and Methods

2.1 Materials

Stattic (#S7024, Selleckchem, USA), Niclosamide (#N3510, Sigma-Aldrich, USA); IL6 (#200-06) and EGF (#AF-100-15) were procured from Peprotech (USA). D-Luciferin Firefly, potassium salt (# L-8220) was from Biosynth (Switzerland). Mouse-anti-STAT3 (#9139), rabbit-anti acetyl-K685 STAT3 (#2523) and rabbit-anti-pY705 STAT3 (#9145) antibodies were from Cell Signalling (USA); rabbit-anti-pS727-STAT3 (#E121-31), mouse-anti-RFP (#ab125244) and rabbit-anti-Cyclin D1 (#ab134175) antibodies were from Abcam. Secondary antibodies like anti-mouse HRP (#ab6728), rabbit- HRP/DAB detection IHC kit (#ab80436) from Abcam and anti-rabbit-HRP (#31460) from Invitrogen. iClick EdU AndyFluor647 cell proliferation kit from Genecopia (USA, #A006). Nanoluc antibody and gene sequence were obtained as a generous gift and Furimazine substrate (#N1110) was procured from Promega Corporation (USA). IVIS Spectrum pre-clinical *in vivo* imaging system equipped with 20 nm bandpass filters covering the range of 500-850 nm and IVIS Lumina II with filters from 500-620 nm was from Perkin Elmer (USA).

2.2 Recombinant plasmid DNA constructions

The Nluc-STAT3 (donor) and Turbo-STAT3 (acceptor) fusion gene vectors were generated by sub-cloning PCR amplified full length STAT3 in-frame in our previously designed pCMV-Nanoluc or pCMV-TurboFP plasmids using C-terminus restriction sites XhoI and SacI. Positive clones were sequence verified for the gene insertion. Respective point mutants of STAT3 on both acceptor and donor plasmids were prepared by sequential site directed mutagenesis approach using primers listed as in **Supplementary Table 1**. For knockdown of endogenous STAT3, a 3'UTR STAT3 shRNA annealed oligo sequence was cloned between HpaI and XhoI site under the U6 promoter of pLL3.7-GFP lentiviral vector as per standardized protocol [28].

2.3 Establishment of cell lines

MCF7 cells were maintained in RPMI-1640 medium supplemented with 10% FBS (US origin, Gibco) and 1% Pen-Strep and incubated at 37°C with 5% CO_2; MDA MB 231 cells were cultured in L-15 medium without $NaHCO_3$ and 10% FBS and 1% Pen-strep in CO_2 free incubator at 37°C as per ATCC recommended condition. MDA MB 231-LucD3H2LN cell line (Perkin Elmer) was used for tumor xenograft study. MCF7 stable cell overexpressing STAT3 point mutations were

generated by transfecting plasmids containing Nluc-STAT3 variants - Wt, Y705F, S727A or K685R described before. Using 500µg/ml Zeocin antibiotic selection, positive clones were selected and verified for Nluc expression by using furimazine substrate. For establishing endogenous STAT3 knockdown lines, first the lentiviral particles were produced using HEK293FT cells co-transfected with pLL3.7-GFP vector containing 3'UTR STAT3 shRNA cassette along with capsid and envelop plasmids in optimized ratio. Lentiviral transduction of MCF7 STAT3 mutant over-expressing clones as well as baseline MDA MB 231 cells were done as per established protocol [28]. GFP positive cells were sorted out as virally transduced cells and knockdown populations were established after three rounds of GFP cell sorting over subsequent passages.

2.4 Live cell luciferase assay

For luciferase assay, live Nluc expressing cells were seeded in triplicates at a density of 5000 or 10000 cells/ well in a black 96 well plate with clear bottom. 50 µl furimazine (1:1000 diluted in medium) substrate was added per well and luminescence photons were measured using IVIS spectrum photon imager in open filter setting.

2.5 Immunoblotting

Cells were seeded at required density for either drug treatment or ligand stimulation experiments. The cells were harvested and lysed in lysis buffer containing: 100mM NaF, 100mM Na_3VO_4, 2mM EGTA, 5mM EDTA, 10µl/ml protease inhibitor and 2µl/ 1ml PMSF, 20mM Tris-Cl pH 7.4, followed by sonication and centrifugation at 14000rpm/30min/4°C. Protein estimation in the supernatant was done using Bradford reagent. 50-60µg protein was loaded and separated in 10% SDS gel followed by transfer in nitrocellulose membrane using semi dry transfer assembly at 15V for 1 hour. Membrane was blocked with 5% non-fat dry milk and incubated overnight at 4□C with primary antibodies for total STAT3 (1:1000 dilution), pS727 STAT3 (1:1000 dilution), pY705 STAT3 (1:500) and K685ac STAT3 (1:500). Following day HRP conjugated secondary antibody incubation was given followed by chemiluminescence detection using ECL substrate kit.

2.6 Cell Survival and Proliferation Assay

For clonogenic cell survival assay, 1000 cells/well were seeded in duplicates in 6 well plates and maintained in normal culture condition. Clones were allowed to form over 14 days, followed by fixing with chilled methanol and staining with 0.5% crystal violet stain. Colonies formed were counted using an illuminated stereo binocular.

EdU AndyFluor647 proliferation kit was used as per the manufacturer's instructions. EdU incubation was given for 16h for MCF7. Images were acquired in LSM780 (Leica) microscope using 633 nm and DAPI filter.

2.7 Quantitative Real Time PCR

Total RNA from control and experimental cells were extracted using RNA extraction mini kit. 2µg RNA per sample was used for preparing cDNA using SuperScript III kit (Invitrogen, USA). GAPDH was used as internal reference control.

Real time PCR was set in Applied Biosystems® QuantStudio™ 7 Flex System. All oligo sequences related to this study are enlisted in **Supplementary Table 1**.

2.8 Immunoprecipitation

For co-immunoprecipitation study MCF7 cells over-expressing Nluc-STAT3 constructs – Wt, Y705F, S727A and K685R were seeded in duplicate at appropriate cell density. Next day the respective acceptor plasmid i.e. Turbo-STAT3-Wt, or any of the PTM mutant Y705F, S727A and K685R was transfected in respective donor cells. 48h post transfection cells were serum starved for 24 hours and stimulated with IL6 (10ng/ml) for 2hr before harvesting the cells. Cells were lysed in ECS lysis buffer (50mM Tris-Cl pH 8.0, 125mM NaCl, 0.5% NP40, 5mM EDTA, 2mM EGTA, 100mM NaF, 100mM Na_3VO_4, 10µl/ml protease inhibitor and 2µl/ 1ml PMSF) and centrifuged at 14000rpm/30min/4°C. From the supernatant collected, protein estimation was done using Bradford reagent. Protein G sepharose beads (GE healthcare) were equilibrated by washing in NETN (20mM Tris-Cl pH 8.0, 100mM NaCl, 0.1% NP40 and 1mM EDTA) buffer thrice at 1000rpm/5min/4°C. The beads were blocked with 5% BSA (in NETN buffer) for 3h/13rpm/4°C. For pull down 1µg protein was incubated with 1µl anti-Turbo antibody (1µg/µl) and 20µl Protein G beads in NETN buffer for overnight/13rpm/4°C. Next day, bound fraction was collected after washing the beads with NETN buffer thrice. Final pellet was re-suspended in 1X denaturing buffer and loaded in 7.5% SDS gel. Immunoblotting was performed with anti-Nluc antibody (1:1000).

2.9 BRET Assay

To perform BRET assays, Nluc expressing cells (Nluc-STAT3 Cl1 to Cl8) were seeded in 12 well plate at a density of 1X10^5 cells/well. Next day, each well was transfected with respective acceptor plasmid i.e. Turbo-STAT3 Cl1 to Cl8 and one set of donor alone cell type was kept separate. 36h post transfection cells were counted and seeded in 96 black well plate at a density of 20,000 cells/well in serum free medium. 24h post serum starvation BRET assay was performed using IVIS spectrum equipped with donor (500±20 nm) and acceptor (640±20 nm) filter sets with or without EGF (100ng/ml) and IL6 (10ng/ml) as ligand and furimazine substrate (1:1000 dilute). For inhibition study, cells are pre-treated with inhibitors for 12h prior to EGF trigger and BRET signal measurement.

BRET ratios were calculated using the following equation [29]:

$$\text{BRET Ratio} = \frac{BL_{\text{acceptor channel}}}{BL_{\text{donor channel}}} - Cf$$

$$\text{Where, } Cf = \left(\frac{BL_{\text{acceptor channel}}}{BL_{\text{donor channel}}} \right)_{\text{Donor alone cells}}$$

2.10 Clinical samples and Ethics Statement

The clinical protocol for IHC analysis of STAT3, pS727 and pY705 was reviewed and approved by the Institutional Ethical Committee III (IEC III). Formalin fixed and paraffin embedded (FFPE) blocks were acquired from breast cancer excision specimens. Waiver of consent from patients was approved by the IEC committee for this protocol. We obtained tumor tissue blocks of triple negative breast cancer (TNBC) cases both diagnostic core biopsy (CB) and paired post NACT (neoadjuvant chemotherapy) for individual patient. A total of 76 tissue samples were collected from patients of age group 24-72 years recruited in between 2012 and 2017. All cases were grade III, invasive ductal carcinoma (IDC), no special type classified as negative for ER, PR and Her2 (triple negative) based on immunohistochemistry. The demographic description of the patient cohort is shown in **Supplementary Table 2**. Majority of the patients received Taxane based Neoadjuvant chemotherapy regimen, which includes docetaxel, paclitaxel, carboplatin either alone or in combination followed by surgery. We also acquired tumor tissue blocks from a few other subtypes of breast cancer i.e. $Her2^+$ (n=5) and ER^+/PR^+ (n=5).

2.11 Immunohistochemistry (IHC)

IHC was performed as per reported protocol [30]. Briefly, 5 µm thick paraffin embedded tissue section was taken on a glass slide and de-paraffinized in xylene followed by rehydration with gradients of alcohol (100%, 90% and 75%). Endogenous peroxidase activity was blocked using 0.3% H_2O_2 solution. Antigen retrieval was performed with sodium citrate pH 6.0 treatment using microwave followed by blocking with blocking reagent provided with the kit (#ab80436 IHC Kit). Primary antibody incubation at respective dilution (1:100 for total STAT3, pS727 STAT3 and 1:50 for pY705 STAT3) was done overnight at 4□C in humidified chamber. After respective HRP conjugated rabbit secondary antibody treatment, DAB detection kit was used for staining and subsequent steps were followed as per the manufacturer's instructions.

2.12 IHC Scoring Methods

For IHC scoring, the Allred method (used for Hormone receptors in breast cancer) was followed where final score is assigned based on both proportion of cells stained (0- no stain,1- less than 1%, 2- 1-10%,3-11-33%,4-35-66 % and 5-67-100% cell stained) and intensity of the staining (0- negative, 1- weak, 2- intermediate and 3- strong stain). A total score is assigned out of 8 [31].

For digital scoring IHC Profiler plugin of the ImageJ software is used. Analysis was performed as mentioned [30, 32]**.** The final score obtained is either 0= negative, 1+ = weak positive, 2+ = positive and 3+ = strong positive. Depending upon the location of the target protein, nuclear or cytoplasmic mode of analysis was selected.

For assigning score of different clinic-pathological parameters, H & E stained tissue samples were used for both core biopsy and post NACT specimens and 10 different field were analysed. Mitotic population score was assigned based on average mitotic count over ten field. 1+: 0-9 mitoses, 2+: 10-20 mitoses and 3+: ⩾20 mitoses per 10 high power field. Apoptosis was graded as Grade 3+/brisk when all the fields showed apoptosis, 1+ when it was seen only in one or two fields and 2+ for the intermediates. Fibrosis assessment was attempted both in core biopsy and excision biopsy samples in spite of the understanding that sampling and NACT may induce variability. Dense fibrosis was when it occupied > 50% of sample, +1 was when < 10% of tumour showed fibrosis. Stromally located tumour infiltrating lymphocytes (sTIL) were graded in multiples of 10 as <10% as negative, 10-20% as +1, 30-40% as 2+, >50% as 3+ [33, 34].

2.13 Breast cancer xenografts and anti-tumour efficacy studies

For developing orthotopic breast cancer tumour model, study protocol was approved by the Institutional Animal Ethical Committee (IAEC). All animal experiments were performed in compliance with the standard protocol and ethical guidelines of the animal facility of the institute. $5X10^6$ luciferase labelled MDA MB 231-LucD3H2LN cells were implanted onto the 5^{th} mammary fat pad of 6-8 weeks old female NOD-SCID mice. When the tumours attained approximate size of $100mm^{3,}$ mice were randomly segregated into two groups; vehicle control (n=4) and treatment (n=4). Drug (Niclosamide, 50mg/kg) was administered via intraperitoneal route in 100µl volume for consecutive 21 days. Tumour growth was monitored non-invasively by injecting 3mg D-luciferin (100µl in saline) via intraperitoneal injection and performing non-invasive bioluminescence imaging using IVIS Lumina II once every week (every 7^{th} day of the treatment). Post treatment schedule, mice were sacrificed and *ex vivo* BL imaging was performed on different organs to monitor metastasis. Tumor volume was measured once in every 7th day using the formula: [length (mm) x $(breadth)^2 (mm)^2$] / 2

2.14 Statistical analysis

All statistical analysis was done using SPSS 10.00 statistical software. Kruskal Wallis H test was applied for non-normal distribution and one-way ANOVA for normal distribution. Chi square test, student t-test, Mcnemar test and post hoc test were applied for comparing variables within the group. Two-tailed p value <0.05 was considered statistically significant.

3 Results

3.1 Noncanonical (pS727 or K685ac) STAT3 activation can operate independent of canonical (pY705) activation in BC cells

Considering the contradictory literature available on mode of STAT3 activation, we decide to investigate whether the two arms of STAT3 activation (pY705 vs. pS727 and/or K685ac) operate in interdependent or independent manner in BC. To address this, expression plasmids for wild type (Wt) or respective PTM mutants (Y705F, S727A and K685R) are designed by fusing with Nanoluciferase (Nluc) reporter gene at 5'end **(Fig. 1A)**. Thereafter, MCF7 STAT3-KD

established cell line is transfected with these expression plasmids and confirmed for fusion gene expression by measuring Nluc activity **(Fig. 1B and Supplementary Fig. 1A-C)**. Expression of intact fusion protein of higher size as indicated by arrowhead in the Wt and mutant STAT3 expressing cells is shown by immunoblotting **(Fig. 1C)**. As expected, Y705F mutant expressing cells show both pS727 and K685ac forms present. In case of K685R, alongside pY705 and pS727 activation, an acetylation band is also seen despite of K685R point mutation, which may be due to non-specific recognition of adjacent acetylated lysine residues at 679, 707 and 709 amino acid position [35]. Surprisingly, in S727A mutant expressing cells, loss of serine site shows total loss of K685ac. To further validate this interesting observation, Wt, Y705, S727 and K685R mutant expressing cells are subjected to either IL6 or EGF ligand treatment for 2h and probed with the same set of antibodies to judge STAT3 activation status **(Fig. 1D-E)**. Results confirm that even in ligand induced condition, Y to F and S to A amino acid conversion in phospho-mutants cause total inactivation of the respective PTM sites. Again, for K to R mutant an acetylation band is observed due to nonspecific recognition of adjacent lysine residues. Further, in case of Y705 loss, no significant change is observed in pS727 levels, but K685ac is increased significantly in the presence of IL6 or EGF induction. Similarly, for K685R mutant an evident increase in pS727 activation is witnessed post ligand stimulation. However, S727 loss causes total inactivation of K685ac site. Interestingly, for Wt, S727A and K685R mutant overexpressing cells, pY705 level increases significantly when treated with IL6 ligand. Taken together it is evident that while Y705 or S727 phospho-activation can take place independently, but STAT3 activation by K685 acetylation residue essentially requires presence of pS727.

3.2 S727A and K685R mutant expressing cells show lower proliferation and survival advantage than Y705F overexpressing cell

As activated STAT3 is known to be a key signaling molecule for cell growth and survival under both normal and oncogenic conditions, how the loss of different STAT3 PTM marks may affect cell proliferation is further investigated. EdU incorporation assay is performed using the clonal MCF7 cell lines. Results show that loss of noncanonical activation marks (S727A and K685R) significantly lower ($p<0.01$ and $p<0.05$ respectively) cellular proliferation ability than cells with Y705 loss or Wt STAT3 **(Fig. 2A)**. The difference in cell proliferation is further evidenced by cell survival assessment, where S727A and K685R clonal cells exhibit significantly lower number of colonies formed ($p<0.001$) when compared to Wt. In comparison though Y705F clone also forms significantly lower number of colonies ($p<0.01$), the number of colonies formed within the same time frame is much higher than the other two PTM mutant lines **(Fig. 2B)**. The size of colonies formed in S727A or K685R are also noticeably smaller than Y705F or Wt clones.

We further judge whether STAT3 PTM status can directly impact important downstream gene targets e.g. Twist1, Socs3, c-Myc, Mcl-1, Bcl-2 and Cyclin D1. With overexpression of Wt construct, an increment in mRNA transcripts level of these STAT3 target genes is noticed ($p<0.01$). However, in mutant clones, more specifically S727A and K685R, expression level of Twist1, Socs3, c-Myc, Bcl-2 and Mcl-1 is much lower than Wt counterpart **(Fig. 2C-F and Supplementary Fig. 2A)**. However, Cyclin D1 transcript and protein expression majorly remained unaltered in both Wt or mutant overexpressing cell lines **(Supplementary Fig. 2B-C)**. These results clearly suggest that more than Y705,

S727 and K685 sites are essential for transcriptional activity of STAT3 for its target genes except for Cyclin D1, whose levels can be maintained with either one of the sites intact.

3.3 pS727 plays pivotal role in STAT3 dimer formation

It is well established in literature that post-activation STAT3 forms homodimer, which is a key step for STAT3 signaling. As a result of homodimer formation its nuclear-cytoplasmic distribution changes as the activated protein moves to the nucleus. Therefore, next we raise the question on how do the PTM specific mutations at the major sites of activation alter STAT3 homodimer formation. To address this, a novel STAT3 phospho-BRET molecular sensor designed by fusing STAT3 (either Wt or a PTM mutant) with either Nluc donor or TurboFP635 acceptor protein is employed. As the Nluc-STAT3 and TurboFP-STAT3 fusion forms dimer, BRET signal increases indicating proximity driven transfer of resonance energy from the donor to the fluorescent acceptor molecule. Therefore, by adding furimazine substrate, a precise measurement of STAT3 activation can be done from live cell environment (model illustration prepared using full length STAT3 sequence from i-Tasser *in-silico* protein structure prediction software) (**Fig. 3A**). To thoroughly investigate the role of individual PTMs in governing the dimerization, we have prepared a library of recombined BRET constructs carrying either Wt or any one of already validated PTM mutants, i.e. Y705F, S727A or K685R or a combination of any two or even all three mutants of STAT3 as shown in **Fig. 3B**. By transfecting these expression plasmid vectors in MCF7 endogenous STAT3 knockdown line, stable clones are established to perform the following experiments. As indicator of STAT3 homodimerization in the presence or absence of IL6, immunoprecipitation is performed by using TurboFP antibody and are probed by Nluc and TurboFP antibody for their binding. In comparison to the Wt, Y705F or K685R cells, S727A mutant shows maximally reduced band intensity of STAT3 homodimers (2.68-fold lower than Wt), thus confirming the importance of this phospho-PTM site in dimerization (**Fig. 3C-D**). Now for the live cell BRET experiment, equal number of clonal cell variants are plated in replicates and for each clone BRET ratio is computed for un-induced, IL6-induced and EGF-induced conditions. For all clones, IL6 ligand treated conditions show significant increase in BRET ratio indicating higher STAT3 dimerization and activation. Further, the data also shows that among all the single mutant, S727 PTM loss (Cl3) has the dramatic drop (~3.5-fold) in BRET ratio when compared to the wild-type clone (Cl1). Whereas, in comparison Cl2 (Y705 loss) or Cl4 (K685 loss) has relatively lesser drop in BRET signal **(Fig. 3E)**. Similar effect is observed in EGF ligand stimulation condition **(Fig. 3F)**. Together, these results indicate that S727 PTM plays a dominant role in STAT3 activation. Further, in Cl5-Cl7, which either retains only one of the PTM sites, the BRET ratio drops further in un-induced or IL6 induced condition. It is also important to note that in all these clones, IL6 ligand stimulation remains primarily ineffective except for Cl5 where ligand stimulation still makes a significant induction in dimerization. However, in Cl7 and 8 (where both Y705/S727 sites are mutated), dimerization is completely prevented as indicated by a negative BRET ratio in un-induced condition and insignificant change under IL6 induction. These observations were equally replicated using another cell line model i.e. MDA MB 231 cells (with endogenous STAT3 KD) **(Supplementary Fig. 3A-C)**. The important role played by the Y705 and S727 phospho-PTM marks in STAT3 homodimerization is thus revealed here.

3.4 Total and phosphoS727 STAT3 expression positively correlates in TNBC subset of BC patient tumour samples

Intrigued by the *in vitro* observations for superior role of pS727 in controlling STAT3 dimerization and activation functions, we next decide to explore STAT3 activation profile in clinical scenario. Previous reports have highlighted significant role of STAT3 in controlling tumour growth of triple negative breast cancer (TNBC). STAT3 is even considered as an emerging target for therapy less TNBCs [36]. Thus, to investigate which pathway of STAT3 activation dominates in TNBCs, a total of 76 TNBC core biopsy samples were acquired to perform immunohistochemistry (IHC) analyses for total STAT3, phosphoY705 and phosphoS727 (**Supplementary Table 2**). Intense to moderate nuclear staining for STAT3 and pS727 and a strikingly weak to moderate nuclear signal for pY705 is observed in majority of cases studied **(Fig. 4A)**. A previously identified positively stained sample of a TNBC case is kept as control for pS727, while an oral cancer case is used as control for total STAT3 and pY705 in each batch of staining. The Allred scoring method (score value 0-4 considered as negative, and 5-8 as positive) employed shows 86% (66/76) of TNBC cases are positive for total STAT3 and more than 92% of STAT3 positive cases are constitutively phosphorylated by its pS727 residue. In comparison, pY705 form is found to be present in only 15% of STAT3 positive cases ($p<0.001$) **(Fig. 4B)**. The observations made using Allred scoring method are also cross-verified by our IHC Profiler digital scoring method. IHC Profiler scoring analysis confirms a strong nuclear STAT3 expression (2+ to 3+ score) associated with pre-dominant pS727 positivity (2+ to 3+ score) in a majority (71/76) of cases. Further, STAT3 positive cases are either found as pY705 negative or weak positive (0, 1+) **(Fig. 4C)**. These results clearly indicate predominant expression of pS727 over its canonical phospho-PTM counterpart in TNBC tumours and this situation prevails in both paired core biopsy and post-NACT specimens analysed. By performing independent correlation analysis of total STAT3 with either pS727 or pY705 in both core biopsy and post NACT specimens, a significantly strong to moderate positive association ($r=0.4987$, $p<0.0005$) between pS727 and total STAT3 expression is obtained. On contrary, pY705 shows insignificant low positive correlation ($r=0.2086$, $p<0.$ 0.0808). Further, the Pearson correlation coefficient value calculated based on Allred and IHC Profiler scoring method do not change significantly (**Table 1**). To confirm if the prominent activation of STAT3 via pS727 is exclusive to TNBC subtype, we extend the IHC scoring analyses in a few additional breast cancer cases representing other major subtypes (n=10). In both $Her2^{+}$ and luminal subtype tissue samples, 90% cases show that the expression of total STAT3 is either negative or weak cytoplasmic, and therefore expectedly phospho-PTM (pY705 and pS727) staining is found negative in them (data not shown).

Further, by comparing the expression of total and the two phospho-PTMs of STAT3 in paired pre- and post-NACT TNBC tissue samples, significant drop in positively stained cases in post-chemo condition is noticed. The percent frequency obtained for total STAT3 drops from 86.2% to 63.2% ($p<0.001$), for pS727 92.1% to 64.4% ($p<0.001$) and for pY705 15.8% to 3.4% ($p<0.01$) respectively **(Supplementary Fig. 4A-C)**. Correlative expression of the three protein markers with various clinico-pathological parameters, e.g. apoptosis, necrosis, mitosis, stromal fibrosis and lymphocytic infiltration, are analysed as shown in **Supplementary Table 3 and Table 4**. Both total and pS727 STAT3 shows significant high mitotic score in both pre- ($p<0.001$ for both markers) as well as post-NACT ($p<0.017$, $p<0.008$ respectively) samples. Stromal lymphocytic infiltration is also found to be higher in post-NACT cases with high STAT3

and pS727 expression (p=0.01, 0.004 respectively). However, other parameters compared, do not show any significant associations in either pre- or post-NACT tissue samples.

3.5 The anti-helminth drug Niclosamide can inhibits the major STAT3 activation signals

The results so far have revealed that presence of any one of the two phospho-PTM marks serves as major catalyst for STAT3 protein activation and drive the downstream signaling in breast cancer. Therefore, to inactivate STAT3 molecule, inhibition of both phospho-PTM sites is important. In an attempt to test various inhibitors of STAT3, we choose niclosamide (NSA) which was previously shown to inhibit pY705 activation and compared NSA drug action with Stattic that is known to prevent docking of STAT3 onto the SH2 domain of activated receptors. Therefore, site-specific inhibition of total and phospho-PTM sites are checked by western blot in MDA MB 231 (**Fig. 5A-B)** and MCF 7 cells (**Supplementary Fig. 5A**). In line of the past reports, our results also show that both Stattic and NSA significantly blocks STAT3 activation via inhibition of phosphoY705 in a dose specific manner, where NSA concentration required is at least 5-fold lower. But additionally, NSA shows specific inhibition of pS727 in both the cell lines, while Stattic was majorly ineffective for this PTM mark even at higher drug concentration. After witnessing site specific inhibition of phospho-STAT3, these two inhibitors are tested for their ability to inhibit STAT3 dimer formation using MDA MB 231 cells expressing STAT3 phospho-BRET sensor. Here also, NSA treatment significantly blocked live cell STAT3 dimer formation (1.78 mBRET ratio at 4µM drug dose, $p< 0.01$) at much lower dose than Stattic (1.73 mBRET ratio at 10 µM drug dose, $p< 0.01$), when compared to the EGF treated controls **(Fig. 5C-D)**. Furthermore, upon EGF stimulation NSA could successfully retain the suppressive activity on STAT3 molecule (2.02 mBRET ratio at 4µM drug dose, $p< 0.01$), for which Stattic failed (3.55 mBRET ratio at 10 µM drug dose, $p< 0.05$). Similar results obtained from MCF 7 cell are shown in **Supplementary Fig. 5B-C**. To verify how STAT3 dimerization inhibition matters in BC cell survival, long term clonogenic survival assessment is done in MDA MB 231 parent and STAT3 KD cells, where both drugs show reduced cell survival in a dose dependent manner ($p<0.01$ for low dose and $p<0.001$ for higher dose). However, the effect of drug induced cell death is seen more prominently in the STAT3 KD condition (3% for 10µM Stattic and 1% for 2µM NSA, $p<0.001$) as compared to the parent counterpart (13.84% for 10µM Stattic and 22.30% for 2µM NSA, $p<0.001$), where again NSA is found to be more effective than Stattic (**Fig. 5E)**. Further, similar assessment is done for the STAT3 PTM mutant overexpressing MCF7 cell line model. Here results show that Wt cells treated with same amount (5uM) of NSA and Stattic drug responds similarly (~50% survival fraction than untreated control), while NSA shows slightly higher efficacy than Stattic (35.33 % vs. 68.77 % respectively) against Y705F mutant **(Fig. 5F)**. In comparison, survival fraction seen in S727A line is 11.61% for NSA and 19.19% for Stattic and for K685R, 18.22 % for NSA and 38.59% for Stattic. Both S727A and K685R cells show much lower survival than Wt or Y705F mutant line. Therefore, unlike Stattic, NSA acts as a dual phospho-PTM blocker, resulting in significantly higher inhibition of STAT3 activation. Hence, based on the evidences gathered here, the new molecular basis of NSA drug function is revealed, which is important towards possible repurposing of NSA as an anti-cancer agent in activated STAT3 positive TNBCs.

3.6 Niclosamide treatment effectively reduces *in vivo* tumour growth and distant metastasis

Thus far, considering the prevalence of phosphoS727 mediated noncanonical STAT3 signaling in clinical cases of TNBCs, we have mechanistically determined independent and critical role of S727 PTM in governing STAT3 dimerization and has shown how NSA treatment can prove to be a better inhibitor option. To further assess the potential of NSA as an anti-cancer drug against TNBCs, MDA MB 231 orthotopic tumour xenograft model is developed coupled with non-invasive bioluminescence (BL) imaging approach. By implanting luciferase labelled MDA MB 231-LucD3H2LN cells orthotopically at the mammary fat pad in immunocompromised mice, tumour growth is monitored using serial BL imaging. Mice with well grown tumours are segregated into control and treatment groups (n=4 each). Treatment group mice receiving 50mg/kg NSA drug consecutively for 21 days show significant inhibition in primary tumour growth as compared to the vehicle control group ($p<0.001$) **(Fig. 6A-B and Supplementary Fig. 6A).** As MDA MB 231-LucD3H2LN cells are also reported to metastasize to bone in particular, we check for distant metastasis spread to both bones and lungs. *Ex vivo* BL imaging of the femur from the same side of the primary tumour confirms no bone metastasis in case of NSA treated cohort **(Fig. 6C)**. Further, NSA treated mice also show significantly lower growth of lung metastatic nodules than the control group **(Fig. 6D)**. However, the body weight for both control and treatment group mice did not show any significant change during the treatment period **(Supplementary Fig. 6B).** Collectively these results confirm *in vivo* anti-cancer efficacy of NSA as potent drug inhibitor against TNBCs.

4 Discussion

Mounting number of evidences strongly place STAT3 at the central node of targeted cancer therapy. Pertaining to multiple PTM sites that can initiate STAT3 signaling, current scenario demands for a better understanding of this oncogenic pathway based on which future drug designing approach can be modified. Hence, to understand the level of interdependent or independent operation of different STAT3 PTMs, clonal cell library overexpressing wild type or mutants at respective PTM sites, individually or in combination, are developed. Upon ligand (IL6 or EGF) stimulation cells devoid of Y705 site show that both pS727 and K685ac expression increases, indicating that STAT3 activation is intact. However, in S727A line, only pY705 expression goes up in stimulated condition and K685 residue acetylation fails to show any induction. Similar is not true for K685R mutant, where both pY705 and pS727 activation is efficiently induced despite K685 acetylation loss. These results clearly indicate that phosphorylation of Y705 and S727 STAT3 can operate independently. Whereas, K685 acetylation is found to be linked with prior pS727 activation. Furthermore, BC cells devoid of S727 and K685 PTM sites also show significantly lower proliferation rate and survival ability than either Wt or Y705F expressing cells. As no such effect on cellular phenotype was apparent in Y705F mutant, it further affirms the possibility that canonical pathway is not the sole driver of STAT3 mediated biological functions in breast cancer cells. Assessing the levels of key downstream transcriptional targets such as Twist1, Socs3, c-Myc, Mcl-1 and Bcl-2 indicates that S727 and K685 sites are more important over canonical Y705, for executing the transcriptional activity of STAT3 molecule inside the cells. Except for Cyclin-D1 whose cellular levels can be maintained even if one of the sites is active or by other common transcription factors. Collectively, these observations clearly specify the important role of noncanonical pathway in controlling STAT3 activation and downstream functions in breast cancer.

Previously it was reported that K685 acetylation [37, 38] and phosphoS727 can independently mediate STAT3 activation and nuclear localization even in the absence of canonical pY705 [17]. Taking the advantage of proximity dependent measurement of *de novo* dimer formation, we developed live cell BRET-phosphorylation assay to define the role played by different STAT3-PTM marks. This is the first time, this study evidently shows that pY705 and pS727 independently mediates STAT3 activation, leading to its dimerization in live cell. In cells with S727 loss, either alone (Cl3) or in combination with other mutants (Cl5, 7 or 8), drastic abrogation in BRET signal indicates precise loss of the proximity between the STAT3 molecules. Further, under condition where cells are incubated with a ligand, Cl3 fails to show improvement in molecular proximity, but Y705 loss (Cl2) or K685 loss (Cl4) alone can still show efficient dimer formation. The observations made by BRET based assessment are further supported by co-IP experiment where S727A mutant clearly shows reduced dimerization All these observations point out critical role of pS727 activation in controlling dimerization of STAT3 upon ligand trigger.

Based on convincing data gathered for independent mode of pS727 mediated STAT3 activation, we next decided to validate this observation at the patient level. Growing number of evidences strongly point toward the association of STAT3 with ER negative tumours [10, 11]. Therefore, we decided to validate our observations in TNBC subset of breast cancer cases. By performing IHC analysis for total, pS727 and pY705 STAT3 in 76 paired core biopsy and post NACT TNBC cases, astonishingly high incidence and expression of pS727 in STAT3 positive cases (86%) intrigued us for further investigation of the underlying biology of noncanonical mode of operation in TNBC. As phospho-PTM expression is correlative to protein activation, pS727 dominance over its canonical counterpart pY705, forms important evidence for noncanonical mode of STAT3 operation in this subtype. In contrary, absence of pY705 and/or pS727 expression in luminal and Her2 high cases (N=10) is expected, as the expression of total STAT3 is either negative or low positive (data not shown). However, conducting a large-scale analysis across all subtypes of breast cancer is important to draw any conclusion. Considering the major role of STAT3 in immune regulation a positive association between total STAT3 and pS727 expression is seen with stromal tumour infiltrating lymphocytes (sTIL) [>30% sTIL] in post NACT samples. This observation is in accordance to previously published reports where an independent association between pSTAT3 expression and tumor infiltrating lymphocytes is observed [39, 40]. However, presence of immune cells in the tumour tissue does not necessarily indicate that they are active. The immune suppressive and tumor microenvironment modulatory functions of STAT3 can inactivate tumor-associated immune cells to cause their functional down regulation [41]. Future studies are required in this direction to further explore the immune modulatory role of STAT3 in the microenvironment of breast cancer tumours. Apart from sTIL, both total and pS727 STAT3 also showed positive association with miotic score in pre- and post-NACT samples. Being a key player in centrosome duplication, high mitotic cell count in STAT3 positive tumours is also justified [42]. Taken together, these clinical observations point towards an important and dominant functional role of pS727 STAT3 PTM site in TNBCs.

Based on the above evidences, it is now perceived that for complete inhibition of STAT3 activity targeting both canonical and noncanonical arm is essential. However, the current drug screening strategy for STAT3 primarily targets pY705 specific inhibition and not pS727 activation [43-46]. Towards finding a solution to this problem, we also test

verify two known STAT3 inhibitors – Stattic [47] and Niclosamide [48, 49]. Our *in vitro* test results show that Niclosamide is more potent than Stattic, as it effectively inhibits both activation marks of STAT3 i.e. pY705 and pS727, reduces STAT3 dimerization ability and thus abrogates the cell survival significantly. This drastic difference in STAT3 inhibitory activity between Stattic and niclosamide can be attributed to their specific mode of action. Stattic is a small non-peptide molecule that prevents the binding of STAT3 SH2 domain with the activated receptor (pTyr motif) and thus inhibits its dimerization and DNA binding ability [47]. Inhibition of STAT3 by this mechanism majorly blocks activation of its pY705 residue, however the pS727 site is still activated by multiple other kinases located in the cytoplasm such as MAPK (mitogen activated kinases), c-Jun, PKC δ (protein kinase C delta) and CDK5 (Cyclin-dependent kinase 5)[50], that are unaffected by Stattic. NSA on the other hand, not only blocks pY705 activation but it also targets other cellular signaling pathways [51]. We believe that NSA with its multipath targeting ability is able to block multiple downstream kinases responsible for pS727 activation thereby causing dual inhibition of STAT3 molecule. Further, in preclinical study, NSA treatment of the orthotopic mammary tumours show significant retardation in the primary tumour growth. Alongside NSA treatment also demonstrates reduced frequency and growth of secondary nodule in distant organs, such as bone and lungs, where 50% or lesser BLI signal is noticed.

5 Conclusion

In conclusion, the present work provides both clinical and experimental evidences for dominant mode of operation by noncanonical STAT3 pathway in breast cancer. Addressing the issue at bench, an in-depth molecular and functional basis is established showing that at least S727 STAT3 PTM plays an independent and pivotal role in STAT3 activation, dimerization and thus promoting its oncogenic activity in BC and more specifically in TNBCs. Therefore, in future IHC based profiling to determine whether canonical or noncanonical arm is actively operating will hold the key for patient stratification and treatment success. In this direction, we also show that anti-helminth drug Niclosamide can be repurposed as a targeted therapeutic agent that significantly inhibits both STAT3 PTM functions **(Fig.7)**. We also believe that with the help of the robust cell-based screening platform developed by using STAT3 phosphorylation BRET sensor, it will provide an opportunity for high throughput screening of drug libraries to discover new or identify existing molecules (like niclosamide) with potential STAT3 inhibitory action.

Acknowledgement

We acknowledge Promega corp. for generously providing us with the nanoluc plasmid and anti-nanoluc antibody as gift. We also acknowledge ACTREC facilities for instrument support.

Funding Sources

We acknowledge DBT bioengineering [REF NO. BT/PR3651/MED/32/210/2011], Govt. of India for funding support through which the study was initiated.

Declaration of Interests

All authors declare no conflict of interest.

Author Contributions

SD -study plan, conduct experiments, data analysis and manuscript drafting; RM –conduct experiments; TS –clinical study plan and data analysis and manuscript review; SM – Statistical analysis of the clinical study; SG –clinical study plan, data analysis and manuscript review; AD –conceived the plan, study plan, data analysis and manuscript writing.

References

[1] H. Yu, H. Lee, A. Herrmann, R. Buettner, R. Jove, Revisiting STAT3 signalling in cancer: new and unexpected biological functions, Nature reviews. Cancer 14 (2014) 736-746.

[2] P.A. Johnston, J.R. Grandis, STAT3 signaling: anticancer strategies and challenges, Molecular interventions 11 (2011) 18-26.

[3] S. Huang, Regulation of metastases by signal transducer and activator of transcription 3 signaling pathway: clinical implications, Clinical cancer research : an official journal of the American Association for Cancer Research 13 (2007) 1362-1366.

[4] R.L. Carpenter, H.W. Lo, STAT3 Target Genes Relevant to Human Cancers, Cancers 6 (2014) 897-925.

[5] H.F. Zhang, R. Lai, STAT3 in Cancer-Friend or Foe?, Cancers 6 (2014) 1408-1440.

[6] H. Lee, A.J. Jeong, S.K. Ye, Highlighted STAT3 as a potential drug target for cancer therapy, BMB reports 52 (2019) 415-423.

[7] M. Berishaj, S.P. Gao, S. Ahmed, K. Leslie, H. Al-Ahmadie, W.L. Gerald, W. Bornmann, J.F. Bromberg, Stat3 is tyrosine-phosphorylated through the interleukin-6/glycoprotein 130/Janus kinase pathway in breast cancer, Breast cancer research : BCR 9 (2007) R32.

[8] K. Banerjee, H. Resat, Constitutive activation of STAT3 in breast cancer cells: A review, International journal of cancer 138 (2016) 2570-2578.

[9] N.G. Chung S.S., Y. Wu, and J.V. Vadgama., STAT3 activation in HER2-overexpressing breast cancer promotes epithelial-mesenchymal transition and cancer stem cell traits, International journal of oncology 44 (2014) 403-411.

[10] H. Lee, P. Zhang, A. Herrmann, C. Yang, H. Xin, Z. Wang, D.S. Hoon, S.J. Forman, R. Jove, A.D. Riggs, H. Yu, Acetylated STAT3 is crucial for methylation of tumor-suppressor gene promoters and inhibition by resveratrol results in demethylation, Proceedings of the National Academy of Sciences of the United States of America 109 (2012) 7765-7769.

[11] Y.T. Yeh, F. Ou-Yang, I.F. Chen, S.F. Yang, Y.Y. Wang, H.Y. Chuang, J.H. Su, M.F. Hou, S.S. Yuan, STAT3 ser727 phosphorylation and its association with negative estrogen receptor status in breast infiltrating ductal carcinoma, International journal of cancer 118 (2006) 2943-2947.

[12] M.A. Aleskandarany, D. Agarwal, O.H. Negm, G. Ball, A. Elmouna, I. Ashankyty, E. Nuglozeh, M.F. Fazaludeen, M. Diez-Rodriguez, C.C. Nolan, P.J. Tighe, A.R. Green, I.O. Ellis, E.A. Rakha, The prognostic significance of STAT3 in invasive breast cancer: analysis of protein and mRNA expressions in large cohorts, Breast cancer research and treatment 156 (2016) 9-20.

[13] H. Sellier, A. Rebillard, C. Guette, B. Barre, O. Coqueret, How should we define STAT3 as an oncogene and as a potential target for therapy?, Jak-Stat 2 (2013) e24716.

[14] J. Srivastava, J. DiGiovanni, Non-canonical Stat3 signaling in cancer, Molecular carcinogenesis 55 (2016) 1889-1898.

[15] S. Shalini Dimri, Abhijit De, Approaching non-canonical STAT3 signaling to redefine cancer therapeutic strategy, Integrative Molecular Medicine 4 (2017) 10.

[16] Z. Wen, Z. Zhong, J.E. Darnell, Jr., Maximal activation of transcription by Stat1 and Stat3 requires both tyrosine and serine phosphorylation, Cell 82 (1995) 241-250.
[17] I. Hazan-Halevy, D. Harris, Z. Liu, J. Liu, P. Li, X. Chen, S. Shanker, A. Ferrajoli, M.J. Keating, Z. Estrov, STAT3 is constitutively phosphorylated on serine 727 residues, binds DNA, and activates transcription in CLL cells, Blood 115 (2010) 2852-2863.
[18] G.S. Lin, Y.P. Chen, Z.X. Lin, X.F. Wang, Z.Q. Zheng, L. Chen, STAT3 serine 727 phosphorylation influences clinical outcome in glioblastoma, International journal of clinical and experimental pathology 7 (2014) 3141-3149.
[19] Z.G. Ouedraogo, M. Muller-Barthelemy, J.L. Kemeny, V. Dedieu, J. Biau, T. Khalil, L.I. Raoelfils, A. Granzotto, B. Pereira, C. Beaudoin, I.P. Guissou, M. Berger, L. Morel, E. Chautard, P. Verrelle, STAT3 Serine 727 Phosphorylation: A Relevant Target to Radiosensitize Human Glioblastoma, Brain pathology 26 (2016) 18-30.
[20] J. Li, G. Cui, L. Sun, S.J. Wang, Y.L. Li, Y.G. Meng, Z. Guan, W.S. Fan, L.A. Li, Y.Z. Yang, Y.Q. You, X.Y. Fu, Z.F. Yan, K. Huang, STAT3 acetylation-induced promoter methylation is associated with downregulation of the ARHI tumor-suppressor gene in ovarian cancer, Oncology reports 30 (2013) 165-170.
[21] R.A. Abhijit De, Akshi Jasani, Engineering Aspects of Bioluminescence Resonance Energy Transfer Systems, in: W. Cai (Ed.), Engineering in Translational Medicine, Springer, London, 2014, pp. 257-300.
[22] E. Powell, W. Xu, Intermolecular interactions identify ligand-selective activity of estrogen receptor alpha/beta dimers, Proceedings of the National Academy of Sciences of the United States of America 105 (2008) 19012-19017.
[23] J. Zou, M. Salarian, Y. Chen, Y. Zhuo, N.E. Brown, J.R. Hepler, J.J. Yang, Direct visualization of interaction between calmodulin and connexin45, The Biochemical journal 474 (2017) 4035-4051.
[24] M. Schroder, K.M. Kroeger, H.D. Volk, K.A. Eidne, G. Grutz, Preassociation of nonactivated STAT3 molecules demonstrated in living cells using bioluminescence resonance energy transfer: a new model of STAT activation?, Journal of leukocyte biology 75 (2004) 792-797.
[25] C. Couturier, B. Deprez, Setting Up a Bioluminescence Resonance Energy Transfer High throughput Screening Assay to Search for Protein/Protein Interaction Inhibitors in Mammalian Cells, Frontiers in endocrinology 3 (2012) 100.
[26] N. Bery, A. Cruz-Migoni, C.J. Bataille, C.E. Quevedo, H. Tulmin, A. Miller, A. Russell, S.E. Phillips, S.B. Carr, T.H. Rabbitts, BRET-based RAS biosensors that show a novel small molecule is an inhibitor of RAS-effector protein-protein interactions, eLife 7 (2018).
[27] S. Dimri, R. Arora, A. Jasani, A. De, Dynamic monitoring of STAT3 activation in live cells using a novel STAT3 Phospho-BRET sensor, Am J Nucl Med Mol Imaging 9 (2019) 321-334.
[28] A. De, S.S. Yaghoubi, S.S. Gambhir, Applications of lentiviral vectors in noninvasive molecular imaging, Methods in molecular biology 433 (2008) 177-202.
[29] S. Dimri, S. Basu, A. De, Use of BRET to Study Protein-Protein Interactions In Vitro and In Vivo, Methods in molecular biology 1443 (2016) 57-78.
[30] S. Chatterjee, R. Malhotra, F. Varghese, A.B. Bukhari, A. Patil, A. Budrukkar, V. Parmar, S. Gupta, A. De, Quantitative immunohistochemical analysis reveals association between sodium iodide symporter and estrogen receptor expression in breast cancer, PloS one 8 (2013) e54055.
[31] A. Qureshi, S. Pervez, Allred scoring for ER reporting and it's impact in clearly distinguishing ER negative from ER positive breast cancers, JPMA. The Journal of the Pakistan Medical Association 60 (2010) 350-353.
[32] F. Varghese, A.B. Bukhari, R. Malhotra, A. De, IHC Profiler: an open source plugin for the quantitative evaluation and automated scoring of immunohistochemistry images of human tissue samples, PloS one 9 (2014) e96801.
[33] S. Loi, D. Drubay, S. Adams, G. Pruneri, P.A. Francis, M. Lacroix-Triki, H. Joensuu, M.V. Dieci, S. Badve, S. Demaria, R. Gray, E. Munzone, J. Lemonnier, C. Sotiriou, M.J. Piccart, P.L. Kellokumpu-Lehtinen, A. Vingiani, K. Gray, F. Andre, C. Denkert, R. Salgado, S. Michiels, Tumor-Infiltrating Lymphocytes and Prognosis: A Pooled Individual Patient Analysis of Early-Stage Triple-Negative Breast Cancers, Journal of clinical oncology : official journal of the American Society of Clinical Oncology 37 (2019) 559-569.
[34] S. Loi, N. Sirtaine, F. Piette, R. Salgado, G. Viale, F. Van Eenoo, G. Rouas, P. Francis, J.P. Crown, E. Hitre, E. de Azambuja, E. Quinaux, A. Di Leo, S. Michiels, M.J. Piccart, C. Sotiriou, Prognostic and predictive value of tumor-

infiltrating lymphocytes in a phase III randomized adjuvant breast cancer trial in node-positive breast cancer comparing the addition of docetaxel to doxorubicin with doxorubicin-based chemotherapy: BIG 02-98, Journal of clinical oncology : official journal of the American Society of Clinical Oncology 31 (2013) 860-867.

[35] Y. Nie, D.M. Erion, Z. Yuan, M. Dietrich, G.I. Shulman, T.L. Horvath, Q. Gao, STAT3 inhibition of gluconeogenesis is downregulated by SirT1, Nature cell biology 11 (2009) 492-500.

[36] J.J. Qin, L. Yan, J. Zhang, W.D. Zhang, STAT3 as a potential therapeutic target in triple negative breast cancer: a systematic review, Journal of experimental & clinical cancer research : CR 38 (2019) 195.

[37] J.J. O'Shea, Y. Kanno, X. Chen, D.E. Levy, Cell signaling. Stat acetylation--a key facet of cytokine signaling?, Science 307 (2005) 217-218.

[38] Z.L. Yuan, Y.J. Guan, D. Chatterjee, Y.E. Chin, Stat3 dimerization regulated by reversible acetylation of a single lysine residue, Science 307 (2005) 269-273.

[39] M. Abou-Ghazal, D.S. Yang, W. Qiao, C. Reina-Ortiz, J. Wei, L.Y. Kong, G.N. Fuller, N. Hiraoka, W. Priebe, R. Sawaya, A.B. Heimberger, The incidence, correlation with tumor-infiltrating inflammation, and prognosis of phosphorylated STAT3 expression in human gliomas, Clinical cancer research : an official journal of the American Association for Cancer Research 14 (2008) 8228-8235.

[40] T. Morikawa, Y. Baba, M. Yamauchi, A. Kuchiba, K. Nosho, K. Shima, N. Tanaka, C. Huttenhower, D.A. Frank, C.S. Fuchs, S. Ogino, STAT3 expression, molecular features, inflammation patterns, and prognosis in a database of 724 colorectal cancers, Clinical cancer research : an official journal of the American Association for Cancer Research 17 (2011) 1452-1462.

[41] H. Lee, S.K. Pal, K. Reckamp, R.A. Figlin, H. Yu, STAT3: a target to enhance antitumor immune response, Current topics in microbiology and immunology 344 (2011) 41-59.

[42] E.J. Morris, E. Kawamura, J.A. Gillespie, A. Balgi, N. Kannan, W.J. Muller, M. Roberge, S. Dedhar, Stat3 regulates centrosome clustering in cancer cells via Stathmin/PLK1, Nature communications 8 (2017) 15289.

[43] Y. Chen, M. Ji, S. Zhang, N. Xue, H. Xu, S. Lin, X. Chen, Bt354 as a new STAT3 signaling pathway inhibitor against triple negative breast cancer, Journal of drug targeting 26 (2018) 920-930.

[44] U. Bharadwaj, T.K. Eckols, M. Kolosov, M.M. Kasembeli, A. Adam, D. Torres, X. Zhang, L.E. Dobrolecki, W. Wei, M.T. Lewis, B. Dave, J.C. Chang, M.D. Landis, C.J. Creighton, M.A. Mancini, D.J. Tweardy, Drug-repositioning screening identified piperlongumine as a direct STAT3 inhibitor with potent activity against breast cancer, Oncogene 34 (2015) 1341-1353.

[45] M. Huang, Z. Chen, L. Zhang, Z. Huang, Y. Chen, J. Xu, J. Zhang, X. Shu, Screening and biological evaluation of a novel STAT3 signaling pathway inhibitor against cancer, Bioorganic & medicinal chemistry letters 26 (2016) 5172-5176.

[46] L.J. Liu, K.H. Leung, D.S. Chan, Y.T. Wang, D.L. Ma, C.H. Leung, Identification of a natural product-like STAT3 dimerization inhibitor by structure-based virtual screening, Cell death & disease 5 (2014) e1293.

[47] J. Schust, B. Sperl, A. Hollis, T.U. Mayer, T. Berg, Stattic: a small-molecule inhibitor of STAT3 activation and dimerization, Chem Biol 13 (2006) 1235-1242.

[48] L. Shi, H. Zheng, W. Hu, B. Zhou, X. Dai, Y. Zhang, Z. Liu, X. Wu, C. Zhao, G. Liang, Niclosamide inhibition of STAT3 synergizes with erlotinib in human colon cancer, OncoTargets and therapy 10 (2017) 1767-1776.

[49] L. Lu, J. Dong, L. Wang, Q. Xia, D. Zhang, H. Kim, T. Yin, S. Fan, Q. Shen, Activation of STAT3 and Bcl-2 and reduction of reactive oxygen species (ROS) promote radioresistance in breast cancer and overcome of radioresistance with niclosamide, Oncogene 37 (2018) 5292-5304.

[50] T. Decker, P. Kovarik, Serine phosphorylation of STATs, Oncogene 19 (2000) 2628-2637.

[51] Y. Li, P.K. Li, M.J. Roberts, R.C. Arend, R.S. Samant, D.J. Buchsbaum, Multi-targeted therapy of cancer by niclosamide: A new application for an old drug, Cancer letters 349 (2014) 8-14.

Figure Legends

Fig. 1. **Independent activation of canonical and noncanonical STAT3 pathway**. **(A)** Schematic representation of expression plasmids showing Nanoluc fusion with Wt–STAT3 or its PTM specific mutants. **(B)** Live cell luciferase activity of stable MCF7-Nluc-STAT3 variant constructs done by adding furimazine substrate in 96-well plates seeded with 5K and 10K cells/well. Bottom graph represents average radiance value calculated for each sample. **(C)** Immunoblot showing intact fusions of Nluc-STAT3 variants in MCF7 stable cells (3'UTR STAT3 KD background) probed for total, pY705, pS727 and K685ac STAT3 using specific antibodies. **(D)** Immunoblot representing differential pattern of STAT3 activation (pS727, pY705 and K685ac) across all the PTM mutants, in response to 2h treatment with IL6 (10ng/ml) or EGF (100ng/ml). **(E)** Bar graphs represent densitometric analysis of normalized band intensities for western blots shown in D.

Fig. 2. **Effect of STAT3 PTM mutants on downstream functional and transcriptional activity in MCF7 cells**. **(A)** Quantitative analysis of percent EdU incorporation in MCF 7 STAT3 mutant construct expressing cells, after 16h of incubation with EdU (n=250 cells). **(B)** Clonogenic cell survival assay of STAT3 Wt and mutant constructs. Photograph of representative well plate with colonies that appeared post 14 days of culturing. Graph shows average number of colonies counted with respect to the parent MCF7 cells. **(C-F)** Charts representing downstream target gene expression in baseline MCF7, Wt and PTM mutant overexpressing clones for TWIST1 **(C)**, SOCS3 **(D)**, c-Myc **(E)** and Mcl-1 (**F).** Graphs represent mean value, error bars represent SEM. Significance levels are indicated as *p<0.05, ** p<0.01, *** p<0.001 and ns non-significant.

Fig. 3. STAT3 phospho-BRET sensor to study STAT3 dimerization in live cell. **(A)** Schematic representation of STAT3 BRET sensor. STAT3 is fused with Nanoluc donor and TurboFP635 acceptor. In the presence of ligand as STAT3 dimerizes, the energy released from catalysis of furimazine substrate by Nanoluc enzyme is successfully transferred to TurboFP635 acceptor protein located in the closest proximity (<10 nm). As a result, TurboFP635 is excited and we get two resultant peaks, one in donor filter and other one in acceptor filter (640 nm). While in the absence of ligand, donor and acceptor molecules are further apart from each other, preventing the energy transfer to the acceptor protein and thus resulting in only donor signal. 3D model of full length STAT3 was developed using i-Tasser in-silico protein structure prediction software. The best model with highest c-score was selected for schematic representation of the STAT3 BRET sensor with modelled N-terminal domain. **(B)** Library of PTM mutants developed for STAT3 BRET vectors, where either individual residues or a combination of them are mutated as indicated by + or – sign against each. **(C)** Co-immunoprecipitation to verify *in vitro* STAT3 dimer formation. Pull down was done using anti-TurboFP antibody followed by probing with anti-Nanoluc and anti-TurboFP antibody. Positive control is cell lysate from Nluc-STAT3 (Wt) overexpressing MCF7 cells. **(D)** Graph representing relative intensity of pull-down band normalized with input control. **(E)** BRET Ratio (milli BRET unit) determined from Cl1-8 cells in absence or presence of 10ng IL6 ligand. **(F)** Wt and single mutant clones (Cl1-4) are further tested for respective BRET ratio in absence or presence of 100ng EGF ligand. Charts represent mean value of triplicate measurements, Y-axis error bars represent SEM. Significance levels are *p< 0.05, **p< 0.01, ***p< 0.001 and ns as non-significant.

Fig. 4. pS727 STAT3 predominates over pY705 STAT3 in TNBC cases. (**A**) IHC photomicrographs of pre- and post-NACT TNBC cases DAB-stained for total STAT3, pS727 and pY705 STAT3. An oral cancer tissue section was used as a positive control for total STAT3 and pY705 STAT3, while a TNBC case was used as a positive control for pS727 staining. Scale bar represent 100µ. (**B**) Distribution of Allred scores (0-8) for total, pY705 and pS727 STAT3 expression in all 76 pre- and post-NACT TNBC samples. (**C**) Similar distribution of digital scoring (0-3) by IHC Profiler method for the same cohort.

Table 1. Pearson's correlation analysis for expression of total STAT3 with pS727 or pY705 in core biopsy and post NACT samples analyzed using two different scoring methods (IHC profiler and Allred scoring).

Fig. 5. **Effect of Niclosamide and Stattic treatment on STAT3 inhibition**. **(A-B)** Western blot of MDA MB 231 cells treated with Stattic (5, 10 and 20µM) for 24h or with NSA (2 and 4µM) for 2, 4, 8 and 12h. Cell lysates were prepared and levels of total STAT3, pS727 and pY705 STAT3 was determined using specific antibodies. **(C-D)** Charts showing milli BRET ratio obtained from MDA MB 231 STAT3 BRET cells after 12h of Stattic or NSA treatment in presence or absence of EGF (100ng) ligand stimulation. **(E)** Chart represents clonogenic survival result for baseline and STAT3 KD MDA MB 231 cells in absence or presence of the inhibitor drugs. (**F**) Chart represents clonogenic survival assay result for MCF7 Wt and PTM mutant clones in response to equal amount (5µM) of Stattic and NSA drug treatment. Each graph represents mean ± SEM. Significance levels are *p< 0.05, **p< 0.01, ***p< 0.001 and ns as non-significant.

Fig. 6. Niclosamide inhibits primary tumour growth and reduces distant organ metastasis in MDA MB 231 orthotopic xenograft model. (A) Representative non-invasive BLI images of control and NSA treated female SCID mice (50mg/kg, i.p route for consecutive 21 days) implanted with luciferase labelled MDA MB 231-LucD3H2LN cells. Imaging was done on every 7th day of the treatment by injecting D-luciferin (3mg via i. p route). Yellow arrowheads indicate primary tumour location on mammary fat pad and arrow indicates distant metastasis appeared in BLI imaging. **(B)** Quantitative analysis of BLI signal (average radiance) from both control and treatment group. Significance level ***p< 0.001. (**C**) Representative *ex vivo* images of excised lungs of mice for both control and NSA treatment groups. Bar graph represents average signal measured from respective lungs. (**D**) Representative *ex vivo* images of excised femur bone of mice for both control and NSA treatment groups. Bar graph represents average signal measured from respective bones. Charts represent mean ± SEM.

Fig.7. Schematic illustration for alternative therapeutic approach to target STAT3 positive TNBC tumours. The two alternate pathways – canonical pY705 and noncanonical pS727 followed by K685 acetylation, can independently activate STAT3 molecules to form a stable homodimer. Thus, targeting STAT3 by blocking these two arms is essential for treatment approach to inactivate STAT3 signaling in tumours. Taking the example of TNBC subtype of BC cases studied here, noncanonical STAT3 activation (pS727/K685 Ac) is predominant than the classical canonical path (pY705). Treatment with inhibitors like Stattic primarily blocks the canonical activation without affecting the pS727 mark. Hence STAT3 signalling still remain active and resulting treatment failure. Whereas, as the study results detailing the mechanism of drug action revealed here, candidate such as Niclosamide can effectively blocks both pS727 and pY705 and thus provide better therapeutic efficacy.

Table 1. Pearson's correlation analysis for expression of total STAT3 with pS727 or pY705 in core biopsy and post NACT samples analyzed using two different scoring methods (IHC profiler and Allred scoring).

Core Biopsy samples				**Post NACT Samples**		
Samples	**N**	**Pearson Correlation Coefficient (r)**	**p Value**	**N**	**Pearson Correlation Coefficient (r)**	**p Value**
(IHC Profiler Method)						
Total STAT3 Vs. pS727	76	**0.4985**	0.0005	58	**0.5497**	0.0005
Total STAT3 Vs. pY705	76	0.187	0.09	58	0.129	0.337
(Allred Scoring Method)						
Total STAT3 Vs. pS727	76	**0.4987**	0.0005	58	**0.4776**	0.0006
Total STAT3 Vs. pY705	76	0.2086	0.0808	58	0.2342	0.1091

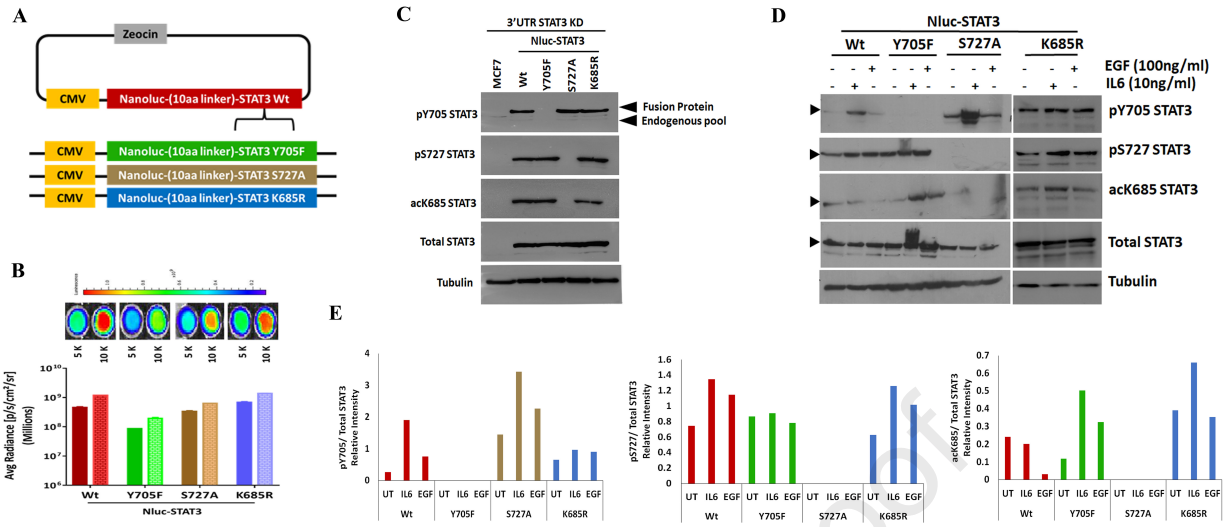

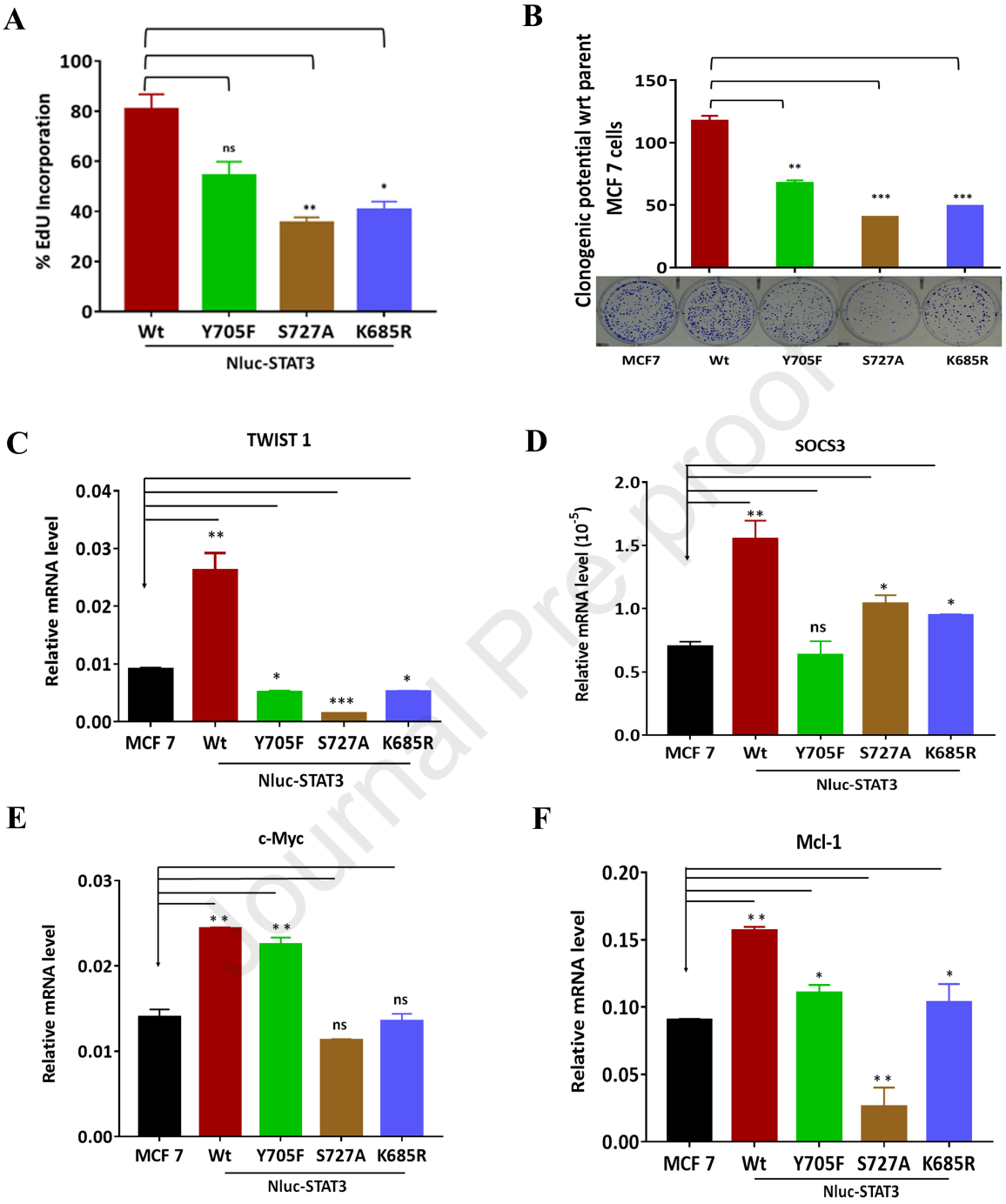
A
% EdU Incorporation
100
80
60
40
20
0
ns
**
*
Wt
Y705F
S727A
K685R
Nluc-STAT3
B
Clonogenic potential wrt parent MCF 7 cells
150
100
50
0
**
***
***
MCF7
Wt
Y705F
S727A
K685R
C
TWIST 1
Relative mRNA level
0.04
0.03
0.02
0.01
0.00
**
*
***
*
MCF 7
Wt
Y705F
S727A
K685R
Nluc-STAT3
D
SOCS3
Relative mRNA level (10-5)
2.0
1.5
1.0
0.5
0.0
**
ns
*
*
MCF 7
Wt
Y705F
S727A
K685R
Nluc-STAT3
E
c-Myc
Relative mRNA level
0.03
0.02
0.01
0.00
**
**
ns
ns
MCF 7
Wt
Y705F
S727A
K685R
Nluc-STAT3
F
Mcl-1
Relative mRNA level
0.20
0.15
0.10
0.05
0.00
**
*
**
*
MCF 7
Wt
Y705F
S727A
K685R
Nluc-STAT3

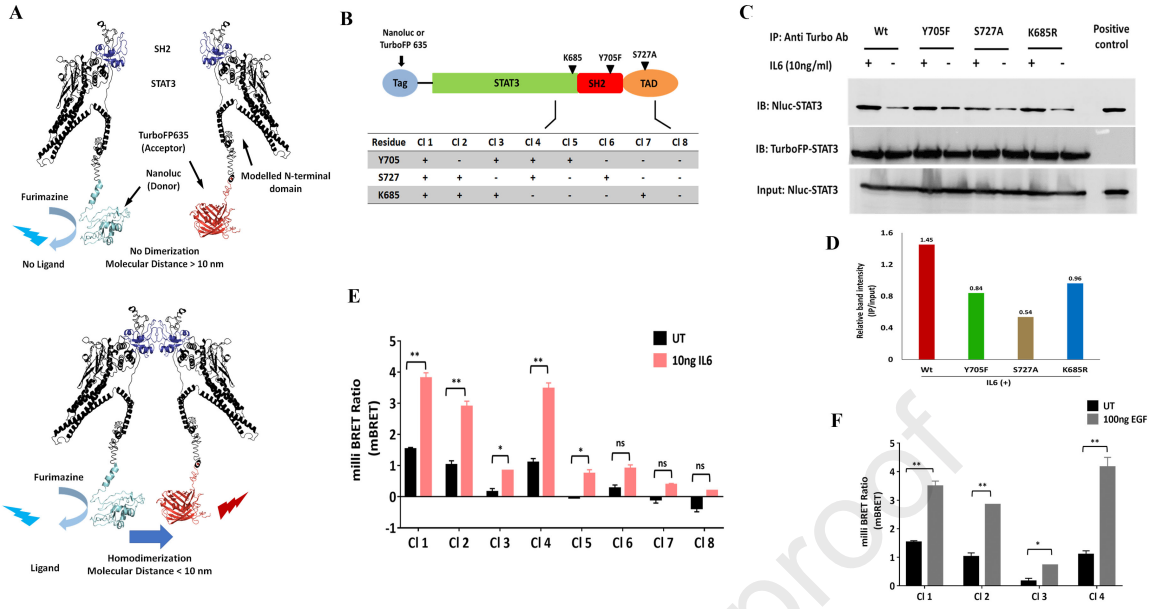

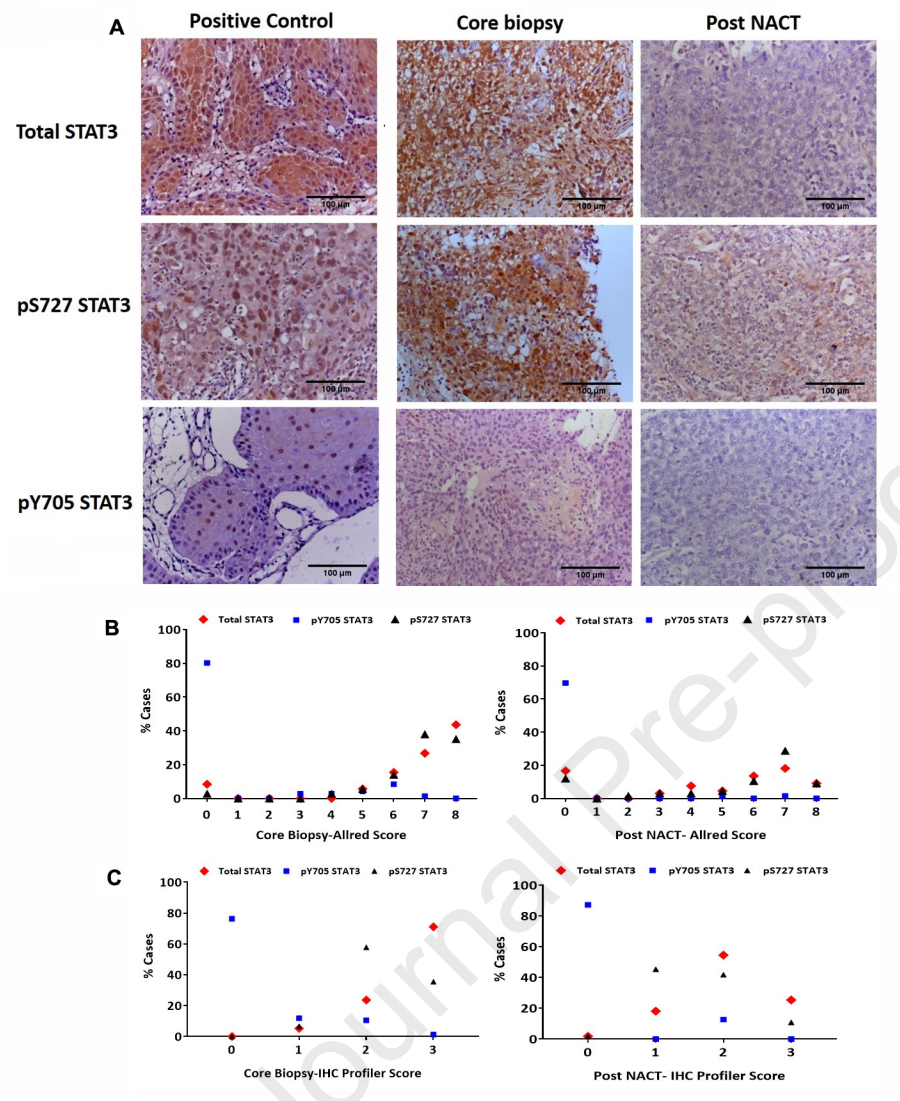

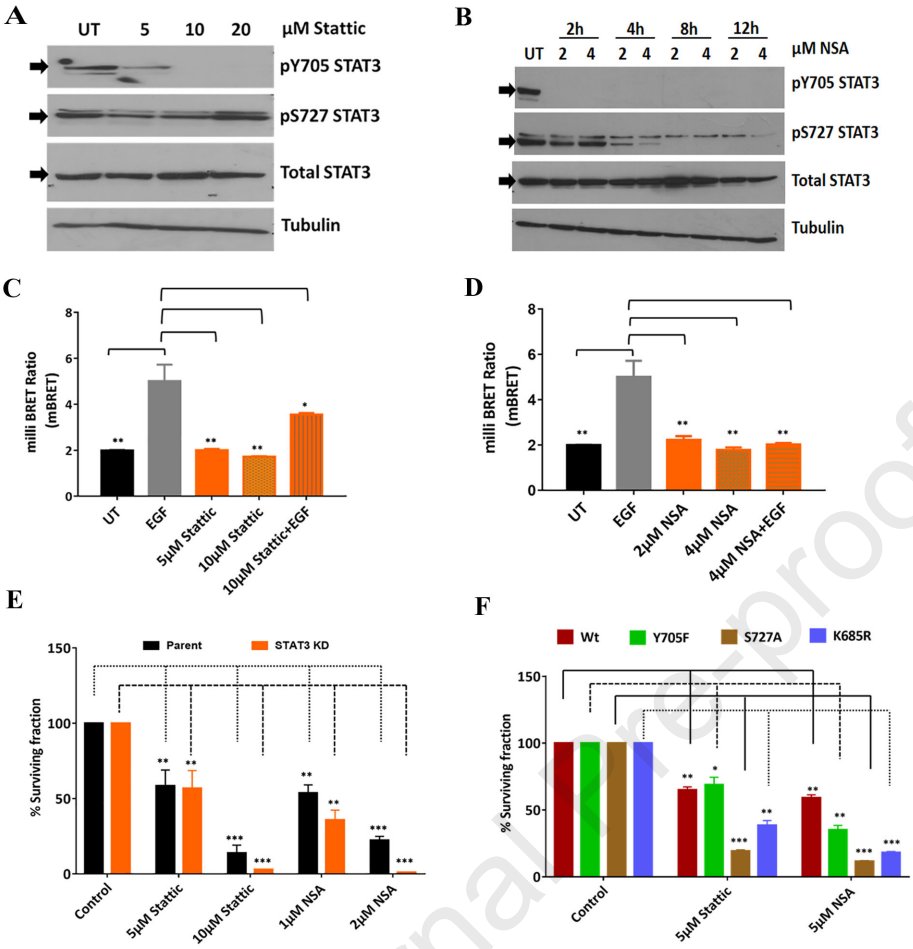

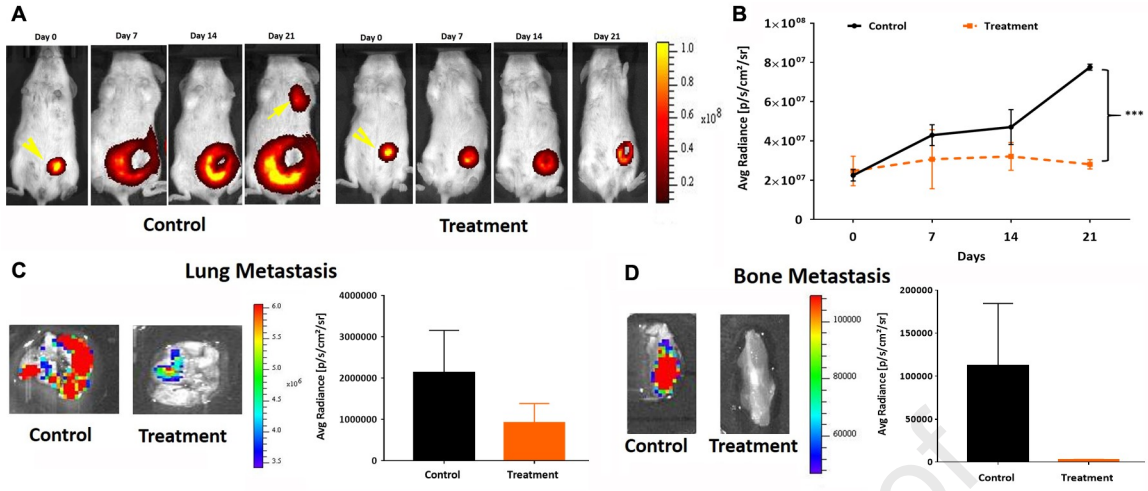

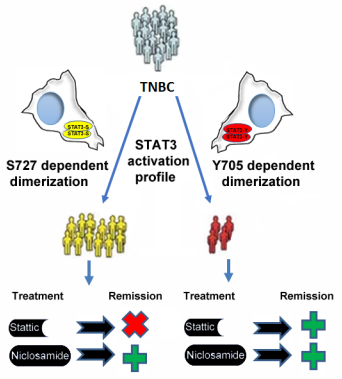

Conflict of Interest

All the authors declare that there are no conflicts of interest.